Electronic Materials Letters (2026) 22:179–186
https://doi.org/10.1007/s13391-025-00609-0

ORIGINAL ARTICLE– NANOMATERIALS

All-Printing Based, Capacitive Pressure Sensors on Paper

Youngjun Cho[1] · Heeyoung Kwack[1] · Taehoon Kim[1] · Kilsoo Lee[1] · Gwangmook Kim[1] · Donyoung Kang[2] · Hyungsuk Lee[2] · Wooyoung Shim[1]

Received: 18 August 2025 / Accepted: 19 October 2025 / Published online: 22 November 2025

Abstract

A fully printed, flexible capacitive pressure sensor was developed using standard desktop inkjet and laser printers on paper. The device consists of printed silver nanoparticle electrodes and a toner–silica nanoparticle composite dielectric layer. A unique microisland-like dielectric structure is formed during laser printing due to heterogeneous particle mixing and selective thermal fusion, resulting in rough surfaces with embedded air gaps. This morphology enhances sensitivity and accelerates response by allowing partial interlocking and compression under applied pressure. The sensor achieves a high sensitivity of 0.08 kPa^{-1} in the low-pressure range (<30 kPa), fast response and recovery times (~50 ms), and maintains mechanical durability over 2000 loading cycles. A 144-pixel sensor array demonstrates scalability, and multifunctional input applications are enabled, including pressure-sensitive trackpads and keyboards where soft and hard touches correspond to distinct commands. This all-printing fabrication approach eliminates the need for microfabrication or complex post-processing, providing a cost-effective, scalable, and versatile method for flexible electronics. The printed pressure sensors offer a promising solution for next-generation human–machine interfaces and customizable paper-based electronic devices.

Graphical Abstract

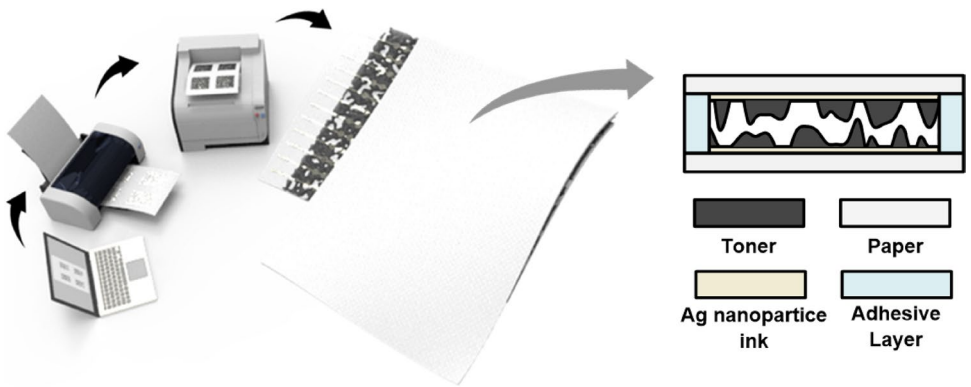

Keywords Capacitive pressure sensor · Paper electronics · Printing · Surface roughness · Input device

1 Introduction

Developing low-cost, high-performance, and flexible devices is of significant interest for a wide range of applications, including flexible displays [1–3], diagnostic tools [4, 5], flexible batteries [6, 7], energy harvesting systems [8, 9], and wearable sensors [10–12]. Among various flexible electronic devices, pressure sensors have attracted considerable

Youngjun Cho, Heeyoung Kwack, Taehoon Kim and Kilsoo Lee contributed equally to this work.

✉ Wooyoung Shim
wshim@yonsei.ac.kr

[1] Department of Materials Science and Engineering, Yonsei University, Yonsei- ro 50, Seoul 03722, Republic of Korea

[2] School of Mechanical Engineering, Yonsei University, Yonsei-ro 50, Seoul 03722, Republic of Korea

attention due to their potential uses in electronic skin [13, 14], patient monitoring [15, 16], and human motion detection [17, 18]. These sensors function as transducers that convert mechanical stimuli into electrical signals, utilizing different transduction mechanisms such as piezoresistive [19, 20], piezoelectric [21, 22], and capacitive modes [23, 24].

Among these, capacitive pressure sensors offer key advantages including high sensitivity, low power consumption, and simple device architecture, as governed by a straightforward electrostatic principle. To enhance the performance of capacitive pressure sensors, significant efforts have been devoted to engineering microstructured or porous dielectric layers [25–27]. These engineered dielectric layers exhibit greater compressibility and a lower effective dielectric constant due to the presence of air, resulting in higher sensitivity compared to sensors with flat dielectric films.

Despite the progress in sensitivity improvement, most approaches rely on costly and complex microfabrication techniques. To address this challenge, alternative low-cost and scalable fabrication strategies have been explored, such as handwriting [28], the use of naturally textured surfaces [29], and printing techniques [30, 31]. Among them, printing stands out as a simple and versatile method for pattern formation on a variety of substrates, including paper and flexible films. Owing to its process compatibility and design flexibility, printing has emerged as a promising approach for the large-scale fabrication of flexible pressure sensors.

Here, we demonstrate capacitive pressure sensors fabricated on commercially available photo paper using standard desktop inkjet and laser printers. We show that the printing process enables the construction of all essential components of the sensor: silver nanoparticle ink is used to print the top and bottom conductive electrodes, while a toner–silica nanoparticle composite film, also printed, serves as the dielectric layer. Notably, we introduce a conceptually new approach for forming a microisland-like dielectric structure via the electrostatic printing mechanism inherent to laser printers. This microstructured layer significantly enhances the sensor's performance.

The resulting device exhibits high sensitivity (0.08 kPa^{-1}), fast response and recovery times (< 50 ms), and excellent mechanical durability over 2000 repeated loading cycles. Moreover, the sensor can be readily integrated into multipixel arrays using the same printing process, demonstrating scalability and versatility for practical applications. To showcase its utility, we further developed functional force-touch input devices, including a printed keyboard and trackpad.

Our approach highlights printing as a simple, all-in-one method for patterning electrodes and forming dielectric layers in capacitive pressure sensors, representing a significant step toward the realization of advanced, low-cost paper-based electronics.

2 Results

The key innovation enabling the formation of a microisland-like, randomly rough dielectric surface lies in a new protocol that leverages the electrostatic digital printing process of a laser printer using a specially formulated toner mixture (Fig. 1a). To make this feasible, silica nanoparticles (SNPs) were added to the commercial toner to prepare a functional mixture suitable for laser printing. In this system, both electrostatic interactions and particle size differences significantly influence the morphology of the resulting composite.

When micro- and nano-sized particles are combined, the homogeneity of the mixture is primarily governed by electrostatic interactions between particles with opposing or similar surface charges. Zeta potential measurements were conducted to evaluate these interactions for the pristine toner (< 10 μm) and SNPs (10–20 nm), as shown in Fig. 1b. Both components were found to carry (–63.04 ± 7.20 mV for toner and −26.25 ± 6.06 mV for SNPs), resulting in mutual electrostatic repulsion, resulting in slightly decreased uniformity. (Fig. 1c). By contrast, when oppositely charged nanoparticles were used, electrostatic attraction promoted spontaneous attachment of SNPs to toner particles, leading to a relatively homogeneous mixture (Figure S1, Supporting Information).

However, the mechanism of laser printers, where toner particles are attached by potential differences, the negative charge of the toner is essential for the laser printing. Furthermore, mixed with positively charged particles, strong electrostatic attraction between toner and charged particle can lead to the formation of large agglomerates. Negatively charged SNPs are suitable for the operating mechanism of laser printing and prevent the formation of large aggregates while exhibiting an appropriate level of uniformity.

Following mechanical mixing, the newly prepared toner mixture was loaded into an empty laser printer cartridge and subjected to a standard laser printing process. This process consists of four main steps (Fig. 1d): (i) the photoreceptor drum is uniformly charged negatively; (ii) a laser beam discharges specific regions, creating a positively charged electrostatic image; (iii) the negatively charged toner particles are attracted to the positively charged regions on the drum; and (iv) the toner is transferred to paper and fused by heated rollers at temperatures up to 170–210 °C.

While the toner-which contains styrene acrylate copolymer (<85%), carbon black (<10%), wax (<10%), and amorphous silica (<3%)-melts and adheres to the paper during fusing, most SNPs, having a melting point above

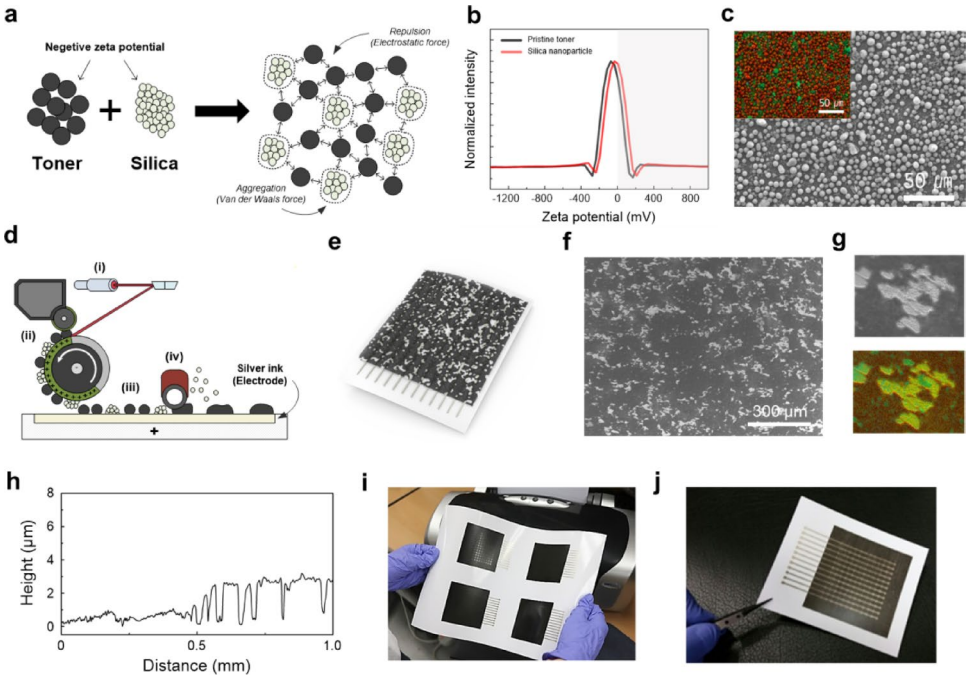

Fig. 1 **a** Schematic illustration of the preparation of toner mixture by adding silica nanoparticles to pristine toner. **b** Zeta potential measurements of pristine toner (black) and silica nanoparticle (red). **c** Typical SEM image of the toner mixture containing silica nanoparticle. Inset is the corresponding EDS mapping image, showing the heterogeneous mixture between pristine toner (red) and silica nanoparticle (green). **d** Schematic illustration for printing process of toner mixture through the electrostatic digital printing process of laser printer. **e** Schematic illustration of the microisland-like dielectric layer printed on the electrode pattern. **f** Typical SEM image of microisland-like dielectric layer surface. **g** A higher-magnification image (top) and corresponding EDS mapping image of the microisland-like dielectric layer surface. The EDS mapping image shows that silver nanoparticle electrode (yellow) is exposed to the outside in between toner (red) and silica (green) composite dielectric layer. **h** Surface profile of microisland-like dielectric layer. **i**, **j** Photograph images of the printed dielectric layer on the patterned electrode, respectively

1600 °C, do not melt or bond to the substrate. As a result, many SNPs are dispersed and lost during printing, and only a fraction remains embedded within the dielectric layer. Consequently, voids form within the dielectric layer, and parts of the underlying AgNP electrode surface are exposed between the toner–SNP composite structures, giving rise to the microisland-like morphology (Fig. 1e and f).

This structure was further validated through energy-dispersive X-ray spectroscopy (EDS) mapping (Fig. 1g), which revealed that most of the exposed regions corresponded to the underlying AgNP electrode, confirming that a substantial portion of SNPs had vanished during the fusing process. Notably, the thermal curing of the AgNP ink also occurred during this process, contributing to a reduction in the sheet resistance of the electrode (Figures S2 and S3, Supporting Information). The average thickness of the printed microisland-like dielectric layer was approximately 2.5 μm, as shown in Fig. 1h. Representative photographs of the printed dielectric layer are shown in Fig. 1i and j. A 144-pixel sensor array was successfully fabricated, covering an area of 4.6×4.6 cm^2,with each pixel occupying approximately 3.14 mm^2.

For the fabrication of the capacitive pressure sensor, two microisland-like dielectric layers with printed electrode patterns were integrated in a parallel-plate configuration (Fig. 2a). A separation layer, embedded between the two microstructured dielectric layers, defines the transverse displacement and air gap. This novel configuration significantly contributes to the sensor's high sensitivity. First, the microisland-like randomly rough surfaces inherently form an air gap between the opposing dielectric/electrode/paper sheets. Second, the addition of an adhesive layer with a thickness of approximately 10 μm helps maintain a consistent air gap. The presence of this compressible air region enhances sensitivity by reducing the pressure required to bring the two layers into contact.

Furthermore, the effective dielectric constant (ε_{eff}) of the sensor increases under applied pressure as the volume fraction of air ($\varepsilon \approx 1.0$) is reduced and replaced by materials with higher dielectric constants-namely, toner ($\varepsilon \approx 2.7$) and silica nanoparticles ($\varepsilon \approx 3.9$). The dielectric constant of the pristine toner was measured and is presented in Figure S4 (Supporting Information). As a result, under normal pressure, the microisland-like surfaces interlock randomly, forming a

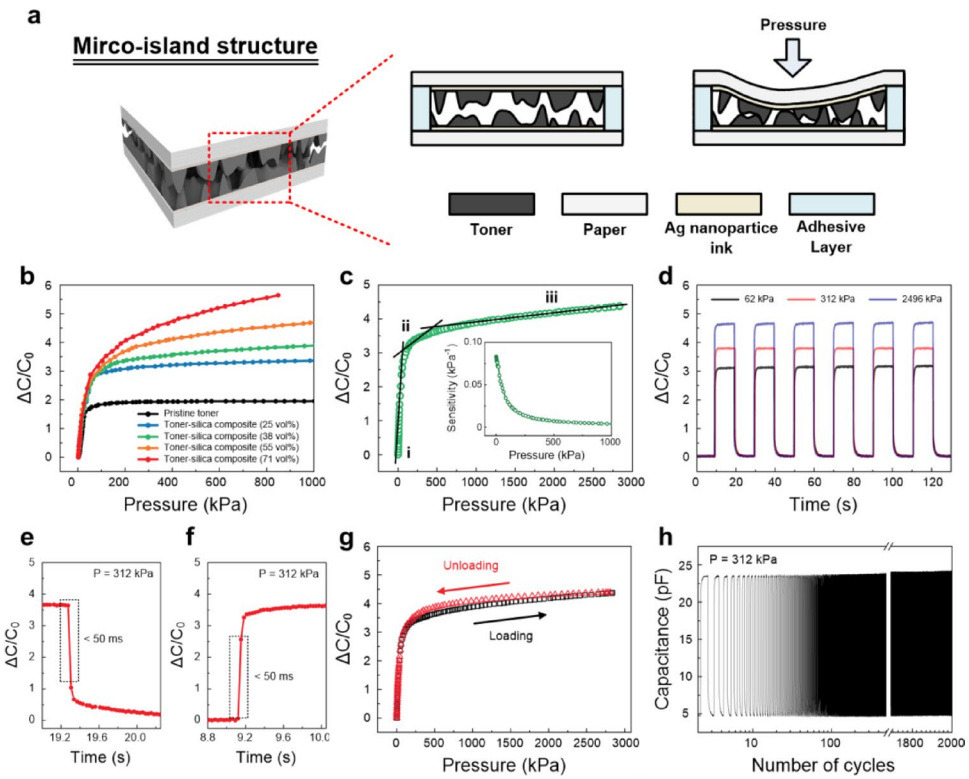

Fig. 2 **a** The schematic illustration for the working principle of the microisland structure based pressure sensor. **b** Capacitive response as a function of pressrue in the range from 0 to 1000 kPa. **c** Capacitive response as a function of pressrue in the range from 0 to 3000 kPa using a device with toner composite film made of a toner mixture containing 38 vol% SNPs. Inset is a plot of sensitivity versus pressure. **d** Capacitive response as a function of time under repeated normal pressure values of 62, 312, and 2496 kPa. **e**, **f** Response and relaxation times for the device under 312 kPa in (e) and (f), respectively. **g** Relative capacitance change from two consecutive linear loading (3000 kPa) and unloading cycles. **h** Stability of capacitive response for the device to a load of 312 kPa over 2000 cycles

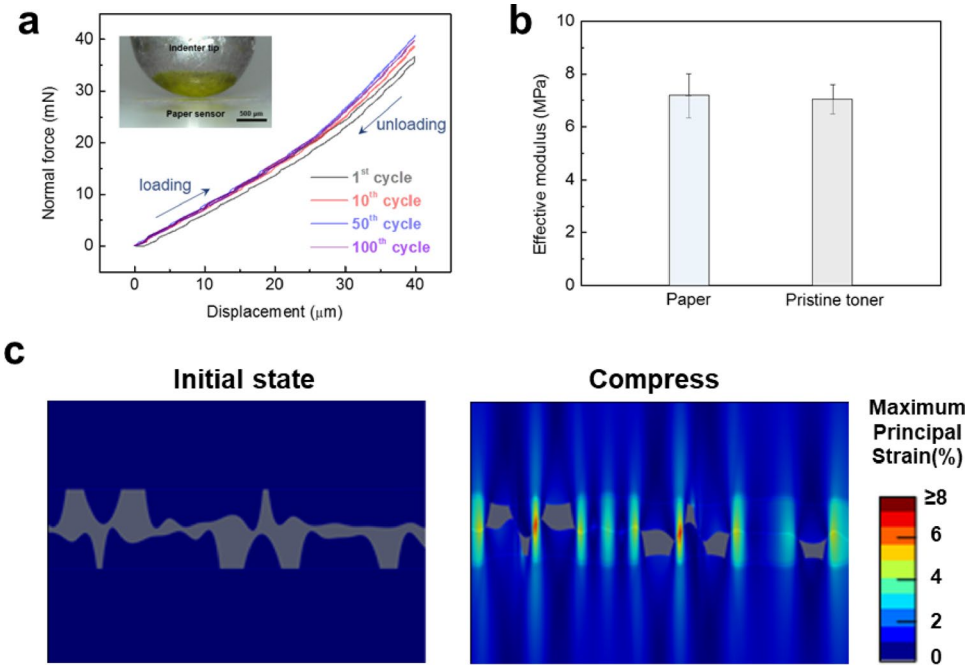

Fig. 3 **a** Repeated normal force-displacement curves using nanoindentation measurement on the pressure sensor, showing the elastic property of the sensor. **b** Effective modulus of the paper (blue bar) and pristine toner (gray bar). **c** Finite element analysis results of all-printing based pressure sensor utilizing microisland-like dielectric layer

dynamic interface that contributes to the sensor's enhanced sensitivity (Fig. 3b).

The sensitivity (S) of a capacitive pressure sensor under normal pressure is defined as $S = \delta(\Delta C/C_0)/\delta p$, where p is the applied pressure, and C and C_0 are the capacitances with and without pressure, respectively. To ensure consistent pressure application, we used a circular force gauge tip with an area of approximately 3.14 mm^2, matching the pixel size.

We analyzed the performance of fully printed pressure sensors fabricated using toner composite films containing varying SNP concentrations (25, 38, 55, and 71 vol%) prior to laser printing. As shown in Fig. 2b, higher SNP concentrations resulted in broader pressure ranges while maintaining

high sensitivity. This trend is attributed to the increased density of microisland structures with increasing SNP content, as illustrated in Figure S5 (Supporting Information).

To ensure dielectric reliability, we printed two microisland-like dielectric layers on the bottom electrode and obtained the capacitance-pressure curve under high pressure (Figure S6, Supporting Information). In these experiments, a smaller circular force gauge tip (≈0.785 mm^2) was used to apply higher localized pressure. Devices with SNP contents above 55 vol% exhibited structural defects in the dielectric layer, leading to undesired conductive paths between electrodes. Notably, no short-circuiting or leakage was observed for devices containing 38 vol% SNPs, even under pressures up to 11 MPa. This indicates that while high SNP concentration is advantageous for increasing sensitivity, it simultaneously adversely affects reliability. We selected the devices containing 38 vol% SNPs for subsequent device fabrication, which exhibited high sensitivity while ensuring reliability even under high pressure conditions.

Figure 3d shows the real-time relative capacitance changes over six cycles at applied pressures of 62, 312, and 2496 kPa. The device demonstrated stable and reproducible sensing performance during repeated loading and unloading. The response and relaxation behaviors are illustrated in Fig. 2e and f. The estimated response and recovery times under a loading pressure of 312 kPa, defined by the time constants of 1–1/e (~63%) for response and 1/e (~36%) for relaxation, were both approximately 50 ms. This fast dynamic behavior is attributed to the mechanically recoverable nature of the paper substrate.

Device hysteresis and long-term reliability were also evaluated. As shown in Fig. 2 g, the sensor exhibited minimal hysteresis during cyclic loading and unloading up to 3000 kPa. Additionally, the device maintained consistent performance over 2000 cycles at 312 kPa without observable signal degradation (Fig. 2 h), demonstrating its robustness for practical use.

The observed elasticity of the device is likely attributed to the mechanically recoverable properties of the paper substrate. To further investigate this, cyclic loading–unloading behavior was examined using nanoindentation measurements. As shown in Figs. 3a and a and 100 repeated loading–unloading cycles were conducted with a maximum displacement of 40 μm and a peak load of 40 mN. During the first cycle (gray curve), a noticeable hysteresis was observed, indicating some degree of irreversible deformation. However, from the second cycle onward, the deformation became predominantly elastic, exhibiting minimal hysteresis and suggesting excellent mechanical recoverability.

To predict the pressure-induced capacitance variations, finite element analysis (FEA) was conducted using the effective moduli derived from the nanoindentation results. The effective moduli of the paper and pristine toner were measured to be 7.17 ± 0.82 MPa and 7.05 ± 0.55 MPa, respectively (Fig. 3b). The simulation results, shown in Fig. 3c, reveal that under applied pressure, the microisland-like dielectric geometry induces local stress concentration at discrete contact points. This leads to the formation of partially interlocked structures between the upper and lower dielectric layers.

These interlocked regions result in the reduction of small air gaps between the microstructured surfaces and consequently increase the overall effective dielectric constant of the device. This enhancement in dielectric constant under pressure leads to improved capacitive sensitivity, validating the mechanical and structural design strategy of the pressure sensor.

To demonstrate the scalability of our pressure sensor for large-area applications, we fabricated a 12 × 12 pixel array, with each pixel having an area of approximately 3.14 mm^2 and a 2 mm spacing between adjacent pixels (Fig. 4a). In such pressure-sensing arrays, spatial acuity is a critical parameter to assess the position-sensing capability. Figure 4b presents a 2D pressure map showing the capacitance change across the array when a pressure of 62 kPa is applied to the center pixel. The temporal response of capacitance at each pixel was also measured, confirming localized sensing behavior (Figure S7, Supporting Information).

Compared to devices fabricated with pristine toner films, those incorporating toner–SNP composite films exhibited enhanced spatial resolution (Fig. 4c). This improvement is attributed to the microisland-like surface morphology, which induces partial interlocking under applied pressure, thereby improving both sensitivity and tactile resolution. In addition, Fig. 4d shows the pressure mapping response when two pixels-spaced four pixels apart-were simultaneously pressed using two pen tips, further highlighting the system's spatial discrimination capability.

Leveraging these improvements, we integrated the sensor into a functional trackpad and full-size keyboard, incorporating 144 and 27 pressure sensors, respectively (Fig. 4e). The inherent pressure-resolving ability of our sensor enables multifunctional input behavior. To demonstrate this, we connected the devices to a data acquisition (DAQ) system capable of measuring capacitive changes and transmitting data to a computer (Fig. 4f). The DAQ system interprets the voltage differences across the capacitive elements, and predefined thresholds were used to distinguish between soft and hard touches.

As illustrated in Fig. 4g and Movie S1 (Supporting Information), soft and hard touches on the trackpad were mapped to drag and double-click operations, respectively. Similarly, on the keyboard, lowercase and uppercase letters

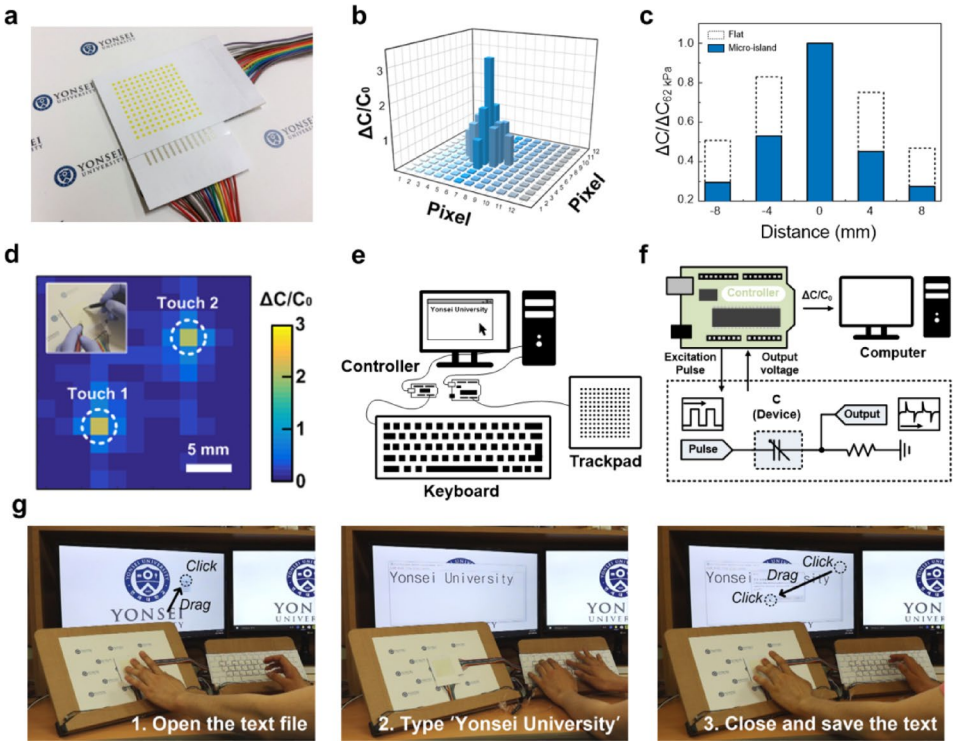

Fig. 4 **a** Photograph of the 12 × 12 multiple-pixel pressure sensor array. **b** Reconstructed 2D pressure map of the change in capacitance, with the center pixel being pressed at 62 kPa. **c** Comparison of cross-talk between the device with toner composite film (blue bar) and pristine toner film (dotted line bar). **d** Capacitance change distribution on the pressure sensor array upon pressing with two pens. **e** Schematic illustration showing the all-printing based input device. **f** A block diagram of capacitance measuring and data acquisition system. **g** Consecutive photographs of using trackpad and keyboard, which have multifunction controlled by magnitude of tactile stimulus

could be entered based on the magnitude of applied pressure, enabling us to successfully type the phrase "Yonsei University" without using the Caps Lock key. These demonstrations underscore the multifunctionality and potential of our all-printed pressure sensor in human–machine interface applications.

3 Discussion

In summary, we developed a fully printed, flexible capacitive pressure sensor on paper substrates using standard desktop inkjet and laser printers. A 144-pixel sensor array was successfully fabricated using a toner–SNP composite to form microisland-like dielectric layers. The resulting sensors exhibited high sensitivity (0.08 kPa^{-1} in the low-pressure regime), fast response and recovery times (< 50 ms), excellent durability over 2000 cycles, and negligible hysteresis. This performance is sufficient to enable various applications, including touch input devices. Importantly, this performance is achieved by a simple and cost-effective process in which all components are printed on flexible paper. Our printing-based approach offers a significant advancement in the trade-off between simplicity and scalability-two factors often considered mutually exclusive in pressure sensor fabrication.

Traditional pressure sensor manufacturing typically requires sacrificing one for the other; however, our method fulfills both criteria through a straightforward, scalable, and cost-effective protocol. Furthermore, there is potential for performance improvements such as sensitivity and uniformity by developing inks and printers, and scalability to various applications can also be expected. This all-in-one printing strategy for forming all critical components of a capacitive sensor is a promising pathway toward next-generation multifunctional electronic devices, including low-cost, customizable pressure-sensitive user interfaces.

4 Method

Fabrication of all-printing based pressure sensor; Commercial aqueous, conductive silver nanoparticle ink (Novacentrix, JS-B25P) was prepared for use with an inkjet printer. The silver nanoparticle ink was printed on photo paper (Formtec, IH-1022) by using an office inkjet printer (model: EPSON Stylus C88+). Then, toner, which consists mostly of styrene acrylate copolymer, was mixed with silica nanoparticle (Sigma-Aldrich, 10–20 nm particle size). After mixing, toner mixture containing 38 vol% silica nanoparticle was then loaded into laser printer (model: Hewlett-Packard, LaserJet Pro 400 color M451dn) catridges and printed on the silver nanoparticle ink printed photo paper. Finally, two half-cells (toner mixture printed paper electrodes) were stacked facing each other with double-sided tape separation layer.

Characterization; Surface morphologies were examined using a JEOL JSM-7001 F field emission scanning

electron microscope (FE-SEM). The Zeta potential of toner and silica nanoparticle was measured using Zeta potential measurement (Otsuka Electronics, Japan). The sheet resistance measurement of silver nanoparticle electrodes before and after thermal curing were conducted using a multimeter (Yokogawa Meters & Instrument corp.). The mechanical properties of the sensor were characterized using custom-made nanoindentation tester, consisting of a load cell (GS0-10, Transducer Techniques), motorized stage (SM2-0803–3 S and SZ-0604–3 S, ST1), and a microscope camera (AM4113, AnMo Electronics Corporation). Capacitance measurements were carried out at 100 kHz frequency with a 1 V AC signal using an Agilent E4980A, Precision LCR Meter. The force applied to the paper pressure sensor was manipulated by a universal manipulator of Teraleader with 0.01 N resolution.

Supplementary Information The online version contains supplementary material available at https://doi.org/10.1007/s13391-025-00609-0.

Author Contributions Y.C., H.K., T.K. and K.L. contributed equally to this work. Y.C., H.K., T.K., K.L.: Conceptualization, Data curation, Investigation, Methodology, Validation, Writing. G.K., D.K.: Conceptualization, Data curation, Investigation, Methodology, Validation. H.L.: Supervision. W.S.: Project administration, Supervision, Review and Writing.

Funding This work was supported by LG Display under the LGD-Yonsei University Incubation Program.

Declarations

Conflict of interest The authors declare no conflict of interest.

References

1. Dai, X., Messanvi, A., Zhang, H., Durand, C., Eymery, J., Bougerol, C., Julien, F.H., Tchernycheva, M.: Flexible Light-Emitting diodes based on vertical nitride nanowires. Nano Lett. **15**, 6958–6964 (2015)
2. Fang, Y., Xia, J., Highly Stretchable: Soft, and clear viscoelastic film with good recoverability for flexible display. ACS Appl. Mater. Interfaces. **14**, 38398–38408 (2022)
3. Sun, J., Chang, Y., Liao, J., Chang, S., Dai, S., Shang, Y., Shan, C.-X., Dong, L.: Integrated, self-powered, and omni-transparent flexible electroluminescent display system. Nano Energy **99**, 107392 (2022)
4. Karnaushenko, D., Ibarlucea, B., Lee, S., Lin, G., Baraban, L., Pregl, S., Melzer, M., Makarov, D., Weber, W.M., Mikolajick, T., Schmidt, O.G., Cuniberti, G.: Light weight and flexible High-Performance diagnostic platform. Adv. Healthc. Mater. **4**, 1517–1525 (2015)
5. Xu, C., Peng, G., Hu, Y., Chen, Y., Xu, Y., Huo, X., Deng, J., Zheng, J., Chen, Y., Zhang, Z., Tao, L., Wu, Z.: A compressible high-sensitivity flexible sensor array for real-time motion artifact detection in magnetic resonance imaging. Nano Energy **131**, 110287 (2024)
6. Chen, Z., To, J.W.F., Wang, C., Lu, Z., Liu, N., Chortos, A., Pan, L., Wei, F., Cui, Y., Bao, Z.A.: Three-Dimensionally interconnected carbon Nanotube–Conducting polymer hydrogel network for High-Performance flexible battery electrodes. Advanced Energy Materials **4**, 1400207 (2014)
7. Li, X., Ling, S., Zeng, L., He, H., Liu, X., Zhang, C.: Directional freezing assisted 3D printing to solve a flexible battery dilemma: Ultrahigh Energy/Power density and uncompromised mechanical compliance. Advanced Energy Materials **12**, 2200233 (2022)
8. Hwang, G.-T., Yang, J., Yang, S.H., Lee, H.-Y., Lee, M., Park, D.Y., Han, J.H., Lee, S.J., Jeong, C.K., Kim, J., Park, K.-I., Lee, K.J.: A reconfigurable rectified flexible energy harvester via Solid-State single crystal grown PMN–PZT. Advanced Energy Materials **5**, 1500051 (2015)
9. An, J., Park, H., Jung, Y.H., Min, S., Kim, D.H., Joe, D.J., Lee, S.-G., Hyeon, D.Y., Je, Y., Seo, H.-S., Jeong, U., Hong, S., Hwang, G.-T., Joung, B., Lee, K.: J. In vivo flexible energy harvesting on Porcine heart via highly-piezoelectric PIN–PMN–PT single crystal. Nano Energy. **121**, 109227 (2024)
10. Feng, Y., Liu, H., Zhu, W., Guan, L., Yang, X., Zvyagin, A.V., Zhao, Y., Shen, C., Yang, B., Lin, Q.: Muscle-Inspired MXene conductive hydrogels with anisotropy and Low-Temperature tolerance for wearable flexible sensors and arrays. Adv. Funct. Mater. **31**, 2105264 (2021)
11. Kim, K.L., Cho, S.H., Lee, J.-B., Kim, G., Lee, K., Lee, S.W., Kang, H.S., Park, C., Ahn, J.-H., Shim, W., Bae, I., Park, C.: Transparent and flexible graphene pressure sensor with Self-Assembled topological crystalline ionic gel. ACS Appl. Mater. Interfaces **15**, 19319–19329 (2023)
12. Fang, Y., Tentzeris, M.M. Inkjet-Printed Flexible Ultrasensitive Chemiresistive Sensors for Aggregation Pheromone of Flour Beetles. Electron. Mater. Lett. **20**, 244–253 (2024)
13. Nela, L., Tang, J., Cao, Q., Tulevski, G., Han, S.-J.: Large-Area High-Performance flexible pressure sensor with carbon nanotube active matrix for electronic skin. Nano Lett. **18**, 2054–2059 (2018)
14. Kim, G., Cho, S., Chang, K., Kim, W.S., Kang, H., Ryu, S.-P., Myoung, J., Park, J., Park, C., Shim, W.: Spatially Pressure-Mapped thermochromic interactive sensor. Adv. Mater. **29**, 1606120 (2017)
15. Chen, L.Y., Tee, B.C.-K., Chortos, A.L., Schwartz, G., Tse, V., Lipomi, J., Wong, D., McConnell, H.-S.P., M. V., Bao, Z.: Continuous wireless pressure monitoring and mapping with ultra-small passive sensors for health monitoring and critical care. Nat. Commun. **5**, 5028 (2014)
16. Kim, T., Kim, G., Kim, H., Yoon, H.-J., Kim, T., Jun, Y., Shin, T.-H., Kang, S., Cheon, J., Hwang, D., Min, B., Shim, W.: Megahertz-wave-transmitting conducting polymer electrode for device-to-device integration. Nat. Commun. **10**, 653 (2019)
17. Zhang, H., Chen, X., Liu, Y., Yang, C., Liu, W., Qi, M., Zhang, D.P.D.M.S.: Film-Based flexible pressure sensor array with surface protruding structure for human motion detection and wrist posture recognition. ACS Appl. Mater. Interfaces. **16**, 2554–2563 (2024)
18. Yao, Y., Dai, H., Ji, M., Han, Y., Jiang, B., Cheng, C. Song, X., Song, Y., Wu. G.: Flexible Strain Sensor Based on AgNWs/MXene/SEBS with High Sensitivity and Wide Strain Range. Electron. Mater. Lett. **20**, 684–693 (2024)
19. Shi, J., Wang, L., Dai, Z., Zhao, L., Du, M., Li, H., Fang, Y.: Multiscale hierarchical design of a flexible piezoresistive pressure sensor with high sensitivity and wide linearity range. Small **14**, 1800819 (2018)
20. Wang, Z., Wang, S., Zeng, J., Ren, X., Chee, A.J.Y., Yiu, B.Y.S., Chung, W.C., Yang, Y., Yu, A.C.H., Roberts, R.C., Tsang, A.C.O., Chow, K.W., Chan, P.K.L.: High Sensitivity, Wearable, piezoresistive pressure sensors based on irregular microhump structures

and its applications in body motion sensing. Small **12**, 3827–3836 (2016)
21. Min, S., Kim, D.H., Joe, D.J., Kim, B.W., Jung, Y.H., Lee, J.H., Lee, B.-Y., Doh, I., An, J., Youn, Y.-N., Joung, B., Yoo, C.D., Ahn, H.-S., Lee, K.J.: Clinical validation of a wearable piezoelectric Blood-Pressure sensor for continuous health monitoring. Adv. Mater. **35**, 2301627 (2023)
22. Park, D.Y., Joe, D.J., Kim, D.H., Park, H., Han, J.H., Jeong, C.K., Park, H., Park, J.G., Joung, B., Lee, K.J.: Self-Powered Real-Time arterial pulse monitoring using ultrathin epidermal piezoelectric sensors. Adv. Mater. **29**, 1702308 (2017)
23. Ha, K.-H., Zhang, W., Jang, H., Kang, S., Wang, L., Tan, P., Hwang, H., Lu, N.: Highly sensitive capacitive pressure sensors over a wide pressure range enabled by the hybrid responses of a highly porous nanocomposite. Adv. Mater. **33**, 2103320 (2021)
24. Joo, Y., Yoon, J., Ha, J., Kim, T., Lee, S., Lee, B., Pang, C., Hong, Y.: Highly sensitive and bendable capacitive pressure sensor and its application to 1 V operation pressure-Sensitive transistor. Advanced Electronic Materials **3**, 1600455 (2017)
25. Zhang, Z., Gui, X., Hu, Q., Yang, L., Yang, R., Huang, B., Yang, B.-R., Tang, Z.: Highly sensitive capacitive pressure sensor based on a micropyramid array for health and motion monitoring. Advanced Electronic Materials **7**, 2100174 (2021)
26. Kang, S., Lee, J., Lee, S., Kim, S., Kim, J.-K., Algadi, H., Al-Sayari, S., Kim, D.-E., Kim, D., Lee, T.: Highly sensitive pressure sensor based on bioinspired porous structure for Real-Time tactile sensing. Adv. Electron. Mater. **2**, 1600356 (2016)
27. Kim, H., Kim, G., Kim, T., Lee, S., Kang, D., Hwang, M.-S., Chae, Y., Kang, S., Lee, H., Park, H.-G., Shim, W.: Transparent, Flexible, conformal capacitive pressure sensors with nanoparticles. Small **14**, 1703432 (2018)
28. Lee, K., Lee, J., Kim, G., Kim, Y., Kang, S., Cho, S., Kim, S., Kim, J.-K., Lee, W., Kim, D.-E., Kang, S., Kim, D., Lee, T., Shim, W.: Rough-Surface-Enabled capacitive pressure sensors with 3D touch capability. Small **13**, 1700368 (2017)
29. Liu, Z., Liang, T., Xin, Y., Huang, J., Liang, J., He, X., Zhang, C., Yang, W., He, X.: Natural bamboo leaves as dielectric layers for flexible capacitive pressure sensors with adjustable sensitivity and a broad detection range. RSC Adv. **11**, 17291–17300 (2021)
30. Shi, H., Al-Rubaiai, M., Holbrook, C.M., Miao, J., Pinto, T., Wang, C., Tan, X.: Screen-Printed soft capacitive sensors for Spatial mapping of both positive and negative pressures. Adv. Funct. Mater. **29**, 1809116 (2019)
31. Cho, Y., Kim, T., Kim, G., Do, H.W., Kim, S.-R., Park, J.-W., Myoung, J.-M., Shim, W.: Three-Dimensional touch device with two terminals. Adv. Mater. **35**, 2305697 (2023)